RESEARCH ARTICLE
ATMOSPHERIC PHYSICS

Earth and Planetary Physics
3: 136–146, 2019
doi: 10.26464/epp2019013

Quasi-90-day oscillation observed in the MLT region at low latitudes from the Kunming meteor radar and SABER

Wen Yi[1,2], XiangHui Xue[1,2,3*], JinSong Chen[4], TingDi Chen[1,2], and Na Li[1,4]

[1]Chinese Academy of Sciences Key Laboratory of Geospace Environment, Department of Geophysics and Planetary Sciences, University of Science and Technology of China, Hefei 230026, China;

[2]Mengcheng National Geophysical Observatory, School of Earth and Space Sciences, University of Science and Technology of China, Hefei 230026, China;

[3]Synergetic Innovation Center of Quantum Information and Quantum Physics, University of Science and Technology of China, Hefei 230026, China;

[4]National Key Laboratory of Electromagnetic Environment, China Research Institute of Radiowave Propagation, Qingdao 266107, China

Abstract: Observations of a quasi-90-day oscillation in the mesosphere and lower thermosphere (MLT) region from April 2011 to December 2014 are presented in this study. There is clear evidence of a quasi-90-day oscillation in temperatures obtained from the Kunming meteor radar (25.6°N, 103.8°E) and Sounding of the Atmosphere using Broadband Emission Radiometry (SABER), as well as in wind observed by the Kunming meteor radar. The quasi-90-day oscillation appears to be a prominent feature in the temperatures and meridional wind tides and presents quite regular cycles that occur approximately twice per year. The amplitudes and phases of the quasi-90-day oscillation in the SABER temperature show a feature similar to that of upward-propagated diurnal tides, which have a vertical wavelength of ~20 km above 70 km. In the lower atmosphere, a similar 90-day variability is presented in the surface latent heat flux and correlates with the temperature in the MLT region. Similar to the quasi-90-day oscillation in temperature, a 90-day variability of ozone (O_3) is also present in the MLT region and is considered to be driven by a similar variability in the upwardly-propagated diurnal tides generated in the lower atmosphere. Moreover, the 90-day variability in the absorption of ultraviolet (UV) radiation by daytime O_3 in the MLT region is an *in situ* source of the quasi-90-day oscillation in the MLT temperature.

Keywords: quasi-90-day oscillation; meteor radar temperatures; SABER temperatures; tides; latent heat release; SABER ozone

Citation: Yi, W., Xue, X. H., Chen, J. S., Chen, T. D., and Li, N. (2019). Quasi-90-day oscillation observed in the MLT region at low latitudes from the Kunming meteor radar and SABER. *Earth Planet. Phys.*, *3*(2), 136–146. http://doi.org/10.26464/epp2019013

1. Introduction

The seasonal variability of winds, temperatures, and tides, such as annual oscillations (AO), quasi-biennial oscillations (QBO), and semiannual oscillations (SAO), are dominant oscillations in the equatorial/low latitude middle atmosphere (Vincent et al., 1998; Gurubaran and Rajaram, 1999; Sridharan et al., 2007; Xu JY et al., 2007; Lu X et al., 2011; Li T et al., 2012). In addition to these long period oscillations, relatively short period oscillations (~10–100 days), known as intraseasonal oscillations (ISOs), also play an important role in the large-scale circulation of the middle atmosphere. Oscillations of ~30–90 days, i.e., Madden-Julian Oscillations (MJOs), were first reported in the tropical troposphere zonal wind by Madden and Julian (1971, 1972) (see the review by Zhang CD (2005) and the references therein). In the MLT region, ISOs were first observed in the zonal wind at Christmas Island (2°N, 157°W) by Eckermann and Vincent (1994), with periods ranging from ~10 to 100 days. Extensive studies were subsequently conducted, from equatorial to high latitudes, to trace the origins of the ISOs in the lower and middle atmosphere; it was suggested that the intraseasonal cycle convection associated with the MJO modulation of the wave activity in the troposphere induces similar periodicities in the MLT region (Eckermann et al., 1997; Lieberman, 1998; Isoda et al., 2004; Miyoshi and Fujiwara, 2006; Kumar et al., 2007; Rao RK et al., 2009; Guharay et al., 2012, 2014).

As mentioned above, the quasi-90-day oscillation is classified as an ISO, but a period of 90 days could be either a seasonal or intraseasonal cycle. The spectral analysis performed by Pancheva et al. (2003) shows that there are periods of ~75 days and ~90 days of variability in MLT zonal mean winds, as observed by meteor radars at middle and high latitudes; however, the period of 90 days in their study was considered to be a fourth harmonic of the AO. Shepherd et al. (2004) analyzed the 7-year mesospheric temperature time series from WIDII/UARS (Wind Imaging Interferometer/Upper Atmosphere Research Satellite) and revealed the presence of a dominant annual ~90- and 60-day oscillation at high northern latitudes. Reid et al. (2014) analyzed 15 years of the hydroxyl (OH) (8–3) 730 nm nightglow emission intensity near 87 km, using filter photometers at the Buckland Park Field Station (34.6°S, 138.6°E) near Adelaide, Australia, and showed that there was 90-day variability in the 00:00 to 03:00 LT and 03:00 to 06:00 LT OH nightglow intensities. Gasperini et al. (2017) reported that a 90-day oscillation in tropospheric convective activity is imprinted

Correspondence to: X. H. Xue, xuexh@ustc.edu.cn
Received 08 NOV 2018; Accepted 18 JAN 2019.
Accepted article online 21 FEB 2019.

into the thermospheric mean winds and DE3. These studies revealed that a variability is evident in the middle and high latitudes of the MLT region, but its characteristics and source mechanisms have not been comprehensively reported and analyzed.

In this study, we present the observations of a quasi-90-day oscillation in the neutral temperatures and winds over a low latitude station (25.6°N, 103.8°E) and preliminarily investigate its source of excitation. A brief description of the observational instruments, dataset, and processing method are given in Section 2, while observations of the quasi-90-day oscillations in temperatures and winds are presented in Sections 3 and 4, respectively. In Section 5, we extensively discuss the exciting mechanism of the quasi-90-day oscillation. We summarize the main results of this study in the final section.

2. Data Sets and Processing Methods

In this study, multiple measurement data from April 2011 to December 2014 are used to investigate the quasi-90-day oscillation in the lower and middle atmosphere over a low latitude region.

2.1 Instruments and Datasets

The Kunming all-sky meteor radar, which has been operating at 37.5 MHz with a peak power of 20 kW since 2008, belongs to the China Research Institute of Radio Wave Propagation (CRIRP), which is part of the Kunming Atmospheric Radar Facility (KARF) located at the Kunming Radio Observatory (25.6°N, 103.8°E) (Xue XH et al., 2013; Yi W et al., 2016, 2018). The daily mean temperatures near 90 km from April 2011 to December 2014 were derived by applying the temperature gradient model technique to data from the Kunming meteor radar (Hocking, 1999; Holdsworth et al., 2006; Yi W et al., 2016). Table 1 shows the number of days in each month that the radar operated during this period. The system parameters of the Kunming meteor radar and temperature gradient model technique were described and discussed by Yi W et al. (2016) and the references therein.

Horizontal winds with resolutions of 1 hour (time) and 2 km (altitude) from April 2011 to December 2014 were observed by the Kunming meteor radar. The wind retrieval technique has been described by Hocking et al. (2001) and Holdsworth et al. (2004). The residual RMS (Root Mean Square) of the hourly horizontal velocity, which is provided by the Kunming meteor radar system, is mostly smaller than 10 m/s. The daily mean zonal and meridional winds were averaged from the zonal and meridional hourly wind data. The tides, including diurnal and semidiurnal tides, were calculated from the zonal and meridional hourly wind data using a harmonic fit method, with a window length of 10 days.

The SABER instrument is carried onboard the TIMED (Thermosphere Ionosphere Mesosphere Energetics and Dynamics) satellite, which was launched in December 2001 (Xu JY et al., 2007). The Microwave Limb Sounder (MLS) instrument is onboard the Earth Observing System (EOS) Aura spacecraft, which was launched in 2004. The MLS observes atmospheric thermal microwave emissions in five spectral regions, from 115 GHz to 2.5 THz. Temperatures are retrieved from bands near the O_2 spectral lines at 118 GHz and 239 GHz (Schwartz et al., 2008). Profiles of temperature and O_3 (retrieved from 9.6 μm emission) observed by SABER (version 2.0) and Aura/MLS (version 4) were selected from a 5°×30° grid centered on the Kunming meteor radar location; SABER temperatures were interpolated and averaged to obtain the daily mean, daytime, and nighttime temperatures at every km of altitude from 20 to 100 km. The daily mean, daytime, and nighttime O_3 data were obtained using the same method used for the temperatures.

2.2 Interpolation Methods

In this study, the quasi-90-day oscillation analyses are based on a daily dataset. The Lomb-Scargle method and harmonic fitting are used to calculate the spectral amplitudes and phase information, respectively. We use Morlet wavelet and cross wavelet analysis (e.g., Torrence and Compo (1998); Grinsted et al. (2004)) to determine how the interested variability varies in the time series. The Lomb-Scargle method (Lomb, 1976; Scargle, 1982) and harmonic fitting are suitable for daily data with gaps; however, the wavelet analysis requires evenly sampled data. Thus, the data gaps are interpolated via the following methods.

First, we choose a data window with a length of 90 days and a shift with a time step of 5 days. When the length of the gap is less than 30 days (approximately 1/3 of the period of interest), the data gaps in this data window are filled using cubic interpolation. Second, due to radar system maintenance there are some gaps larger than 30 days (months marked with red in Table 1) in the Kunming meteor radar data. These data gaps are filled with random values that have the same means and standard deviations, with a window length of 15 days, as the same days in subsequent years (e.g., Luo Y et al., 2001).

3. Quasi-90-day Oscillation in the Middle Atmospheric Temperatures

Because the Kunming meteor radar is located at low latitudes, it suffers from the diurnal variation of meteor occurrence. The meteor echoes are concentrated mainly from 16:00 to 06:00 UT (i.e., 00:00–14:00 LT); therefore, the Kunming meteor radar temperatures are subject to local morning tidal modulation (Yi W et al.,

Table 1. Number of operational days in each month for the Kunming meteor radar

	Jan	Feb	Mar	Apr	May	Jun	Jul	Aug	Sep	Oct	Nov	Dec
2011	–	–	–	16	31	28	31	31	30	31	30	30
2012	30	13	26	30	31	22	11	4	21	31	30	31
2013	31	28	29	30	31	30	31	19	–	–	30	31
2014	31	28	24	30	31	30	31	31	30	31	30	31

2016). Figure 1 presents the daily temperature estimated using the Kunming meteor radar, and the 16:00–06:00-UT-averaged daily temperature obtained from SABER. The daily Kunming meteor radar temperatures are in good agreement with the daily SABER temperatures; approximately 73% and 94% of the differences between them were less than 10 K and 20 K degrees, respectively. Figure 1b shows the comparison of the monthly mean temperatures obtained from the Kunming meteor radar and SABER. It is clear that the monthly mean temperature derived from the Kunming meteor radar is very consistent with the SABER monthly mean temperature; the difference averages approximately 4 K degrees (Yi W et al., 2016).

Figures 2a and 2b show Lomb-Scargle periodograms of the temperatures obtained from the Kunming meteor radar and SABER

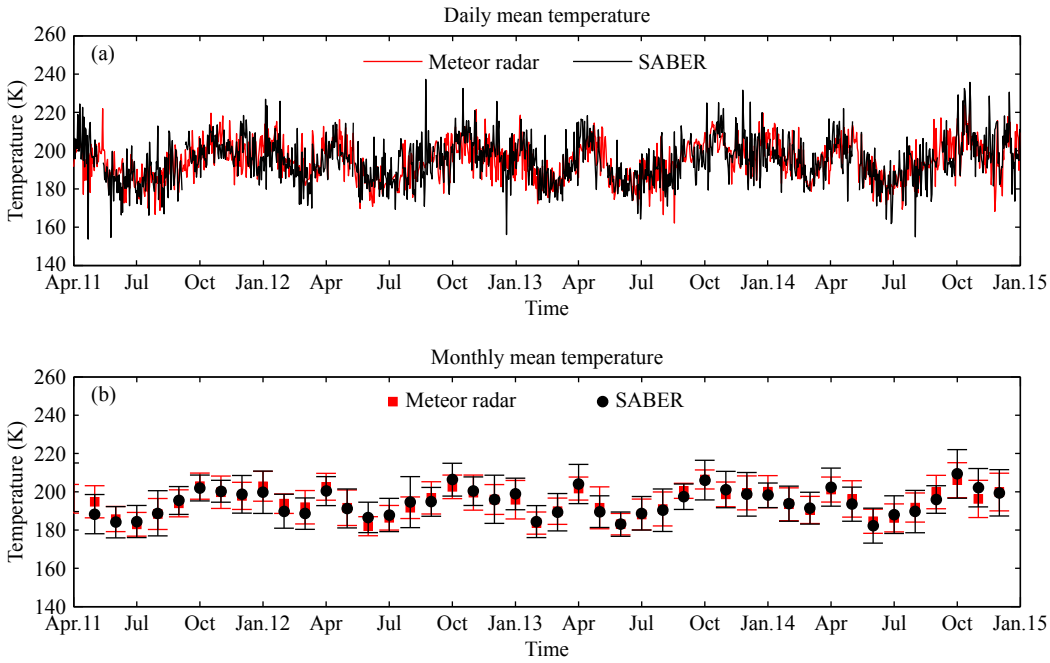

Figure 1. (a) Daily temperatures near 90 km, estimated using the temperature gradient model technique, comparing the Kunming meteor radar temperatures with the SABER temperatures near 90 km; (b) Same as (a) but for the monthly mean temperature. Vertical bars indicate the standard deviations of the monthly mean temperatures.

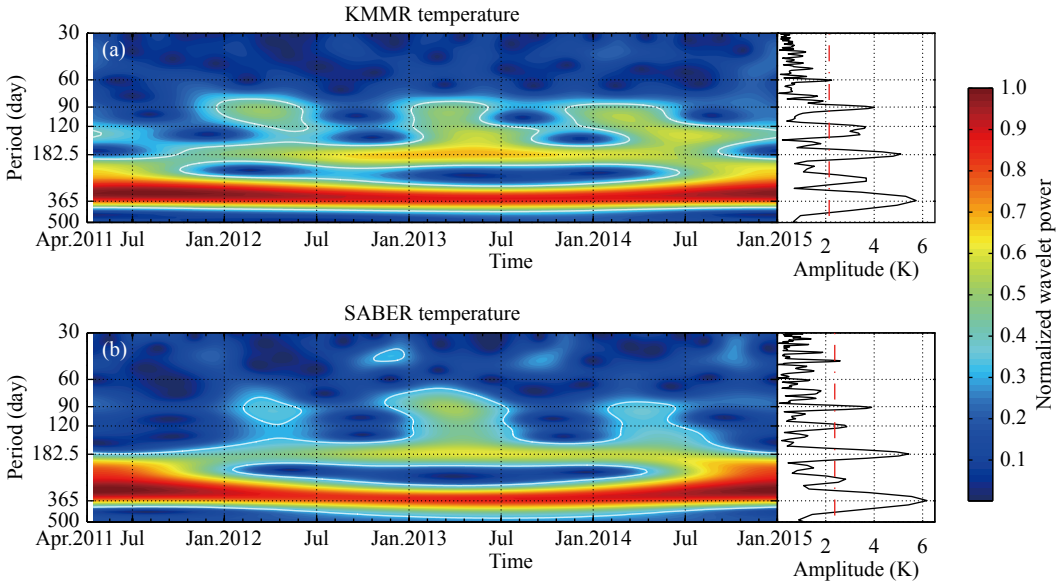

Figure 2. Wavelet spectrum for the (a) Kunming meteor radar and (b) SABER temperatures. The white solid contours denote the regions of the wavelet spectrum above the 95% confidence level. Lomb-Scargle periodograms for the Kunming meteor radar temperatures and SABER temperatures are on the right-hand side for reference; the red dashed lines on the Lomb-Scargle periodograms indicate the 95% confidence level.

for periods of 30 to 500 days. In general, the spectral peaks of the meteor radar temperatures that have confidence levels higher than 99% agree well with the SABER observations. The quasi-90-day oscillation is the third largest oscillation; the amplitudes of the meteor radar temperature and the SABER temperature are both 4.2 K degrees. The AO of approximately 365 days is the largest oscillation; the amplitudes are 5.7 K degrees for the meteor radar temperature and 6 K degrees for the SABER temperature. The SAO of approximately 182.5 days is the second largest oscillation, with amplitudes of 5 and 5.2 K degrees for the meteor radar temperature and the SABER temperature, respectively. Finally, the amplitudes of the terannual oscillation (TAO) of approximately 120 days are 3.5 and 2.67 K degrees, respectively.

The 90-day period is approximately that of the fourth harmonic of the AO or the second harmonic of the SAO (Pancheva et al., 2003). Shown in Figure 2 are the Morlet wavelet spectra, calculated from 30 to 500 days for the meteor radar temperatures, and the SABER temperatures. The wavelet spectra reveal that the quasi-90-day oscillation appears in the first half of the year for approximately two cycles, unlike the SAO and AO in the meteor radar and SABER temperatures; this observations strongly suggests that the quasi-90-day oscillation must be caused by a geophysical mechanism rather than the beat frequency of the AO or SAO. In addition to the 90-day oscillation in temperature, we also find a 90-day oscillation in mesopause density estimated by the Kunming meteor radar (Yi W et al., 2018).

For a better illustration, Table 2 shows the harmonic fit results of the Kunming meteor radar and SABER temperatures. The phases (first maximum after Jan. 1, 2012) of the AO, SAO, TAO and the quasi-90-day oscillation occur on December 7±7 days, April 20±4 days, May 2±3 days and January 15±2 days in the meteor radar temperatures, respectively, and December 3±10 days, April 22±6 days, Apr 23±7 and January 15±4 days in the SABER temperatures, respectively (Yi W et al., 2016).

Notably, the temperatures obtained from the Kunming meteor radar and SABER both exhibit a very large warming in spring (late April) each year. Combining the results of Table 2, we infer that the late April warming is caused by the superposition of the SAO, the next cycle of the quasi-90-day oscillation (i.e., on April 16), and the TAO because the phase maxima of all these oscillations occur simultaneously at that time (Yi W et al., 2016). This finding reveals that the quasi-90-day oscillation plays a significant role in the seasonal and intraseasonal variability of MLT temperature at low latitudes.

To investigate further the characteristics of the quasi-90-day oscillation in the middle atmosphere temperature, we extracted the amplitudes and phases of the quasi-90-day oscillation in the daytime and nighttime and the daily mean temperatures obtained from the SABER measurements over Kunming between altitudes of 40 and 100 km. Figures 3a, 3b and 3c show the quasi-90-day oscillation that is generally present in the middle atmosphere. The amplitudes of the quasi-90-day oscillation increase roughly with altitude. Meanwhile, we found that throughout most of the altitude range the quasi-90-day oscillations have larger amplitudes in daytime temperatures than in nighttime temperatures.

Figures 3e, 3f and 3g show the downward propagation of the phases of the quasi-90-day oscillation; these data appear to reveal that the quasi-90-day oscillation propagates upward from the lower atmosphere with a vertical wavelength-like characteristic of ~20 km above 70 km. However, the quasi-90-day oscillation could not propagate upward directly from the lower atmosphere to the middle atmosphere because of its slow phase velocity (Eckermann and Vincent, 1994; Eckermann et al., 1997; Huang KM et al., 2015). On the contrary, high-frequency wave activities, such as tides, gravity waves, and ultrafast Kelvin waves, with high phase speeds, possibly propagate upward to the MLT region. Many studies have investigated the relationship of the ISOs between the lower and middle atmosphere since the ISOs in the MLT region (MLT-ISOs) were first observed in the zonal wind by Eckermann and Vincent (1994). They proposed that the ISOs in the tropical troposphere convection produce corresponding intraseasonal variability in the intensity of tides, ultrafast Kelvin waves, and gravity waves that reach the MLT region (Eckermann et al., 1997; Lieberman, 1998; Isoda et al., 2004; Miyoshi and Fujiwara, 2006; Kumar et al., 2007; Guharay et al., 2012, 2014). Recently, Yang W et al. (2017, 2018), using the Specified-Dynamic Whole Atmosphere Community Climate Model (SD-WACCM), simulated the response of the mesospheric migrating diurnal (DW1) tides to the MJO and found that the MJO can affect the tidal forcing by modulating both solar insolation absorption and latent heat release in the equatorial troposphere.

Figures 3d and 3h show the GSWM-09 (global-scale wave model, Hagan et al. (1995)) of the diurnal tide of the temperature in January and July between altitudes of 20 and 100 km over (27°N, 105°E). The GSWM-09 reveals that the diurnal tidal amplitudes grow rapidly with altitude, and the vertical wavelength of the propagating diurnal tides is ~30 km above 70 km. Zhang XL et al. (2006) indicated that the vertical wavelength of the upward propagated diurnal tide in SABER temperatures (~22 km) is significantly shorter than in the GSWM (~30 km). Mukhtarov et al. (2009) extracted the global vertical structure of the diurnal tide in SABER temperatures and indicated that the diurnal tide propagated upward from the lower to upper atmosphere with two differ-

Table 2. Results of harmonic fits to the temperatures estimated from the Kunming meteor radar and SABER temperatures

Period (days)	91	122	182	365
Meteor radar phase (day) (first max after Jan. 1, 2012)	15±2 Jan. 15 Winter	123±3 May 2 Spring	111±4 Apr. 20 Spring	342±7 Dec. 7 Winter
SABER phase (day) (first max after Jan. 1, 2012)	18±4 Jan. 18 Winter	114±7 Apr. 23 Spring	113±6 Apr. 22 Spring	338±10 Dec. 3 Winter

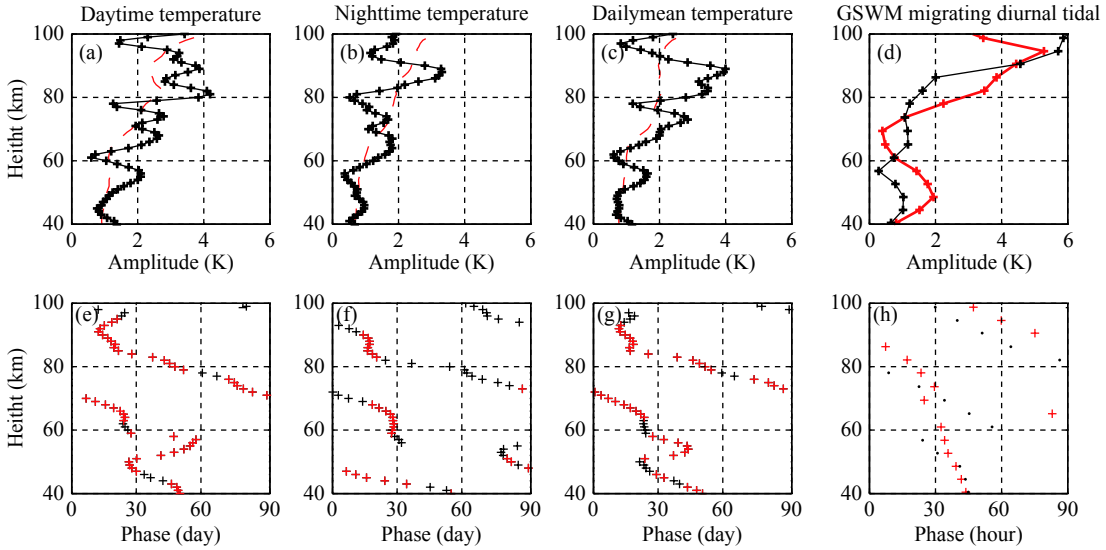

Figure 3. (a), (b) and (c) Amplitude-height profiles of the quasi-90-day oscillation for the SABER daytime, nighttime, and daily mean temperatures, respectively. The black pluses indicate the Lomb-Scargle periodogram amplitudes of the quasi-90-day oscillation at each altitude; the red line indicates the 95% confidence level; (d) Amplitude-height profiles of the temperature in January (black plus line) and July (red plus line) obtained from the GSWM-09 migrating diurnal tidal data at (27°N, 105°E); (e), (f) and (g) Phase-height profiles of the quasi-90-day oscillation for the SABER daytime, nighttime, and daily mean temperatures, respectively. The phase of the quasi-90-day oscillation at each altitude is obtained from the harmonic fit; the red pluses indicate that the amplitude was higher than the 99% confidence level; (h) Same as (d), but for the phase-height profiles.

ent vertical phase gradients in different altitude ranges, i.e., 55–70 km and 70–110 km. The vertical phase gradient of upward propagated diurnal tides in the range of 55–70 km is larger than that in the range of 70–110 km; moreover, two wave cycles of diurnal tides with a vertical wavelength of ~20 km are clearly visible above 70 km.

Coincidentally, the vertical phase structure and wavelengths of ~20 km with two wave cycles above 70 km are similar to the results derived by Mukhtarov et al. (2009), as shown in Figure 3f, i.e., in the nighttime SABER temperature. Moreover, the amplitude of the quasi-90-day oscillation has a trend similar to that of the tidal amplitude obtained from the GSWM-09, as shown in Figure 3d. Combining the above results, we, therefore, infer preliminarily that the quasi-90-day oscillation may modulate the intensity of the diurnal tides in the lower atmosphere and then propagate upward to the middle atmosphere with the diurnal tides.

4. Quasi-90-day Oscillation in MLT Wind

We also use the horizontal wind field observed by the Kunming meteor radar to examine the quasi-90-day oscillation in the MLT region. Figures 4a and 4b show the monthly mean zonal and meridional winds between altitudes of 80 and 100 km. The velocities of daily mean zonal and meridional winds are smaller than 50 m/s and 25 m/s, respectively. The daily mean zonal winds are dominant, with annual variations above 86 km (here, we show the wind fields only above 80 km because the wind fields below 80 km observed by the Kunming meteor radar are not as continuous as those above 80 km), having a strong eastward wind flow with maximum of approximately 50 m/s in summer and a westward wind flow with a maximum of approximately 25 m/s in winter above 86 km. Note that there is only semiannual oscillation at 80–86 km because the phase reversal of annual variations just happens in this region. Li N et al. (2015) analyzed 3 years of wind field data from August 2008 to August 2010 observed by the Kunming medium frequency (MF) radar and reported similar circulation of zonal mean winds as those from Kunming meteor radar observations; however, a slightly different feature is the semiannual variation that presents at 86–88 km. The daily mean meridional winds are dominant with semiannual variations above 84 km, having a strong equatorward wind at a maximum of 23 m/s in spring and autumn above 94 km; then, the annual variation dominates below 84 km, with a poleward wind at a maximum of 25 m/s in winter.

Figures 4c and 4d show Lomb-Scargle periodograms of the daily mean zonal and meridional winds between altitudes of 80 and 100 km. The daily mean zonal winds showed mainly the AO above 88 km and the SAO from 80 to 86 km; the amplitudes of AO and SAO reach maxima as large as 13.7 m/s and 11.1 m/s at approximately 92 and 80 km, respectively. In addition to the AO and SAO, the daily mean zonal winds also show short-term variations, including the 120-day, 90-day and 60-day oscillations; however, these variations are very weak. The quasi-90-day oscillation presents in zonal wind at 84 km with an amplitude of approximately 3 m/s.

The daily mean meridional winds show mainly the SAO above 84 km and the AO below 84 km; the amplitudes of SAO and AO reach maxima as large as 8.3 m/s and 10.1 m/s at approximately 98 km and 80 km, respectively. In addition, the quasi 120- and 90-day oscillations are present in meridional winds; the amplitudes of the quasi-90-day oscillation reach a maximum as large as 3.4 m/s

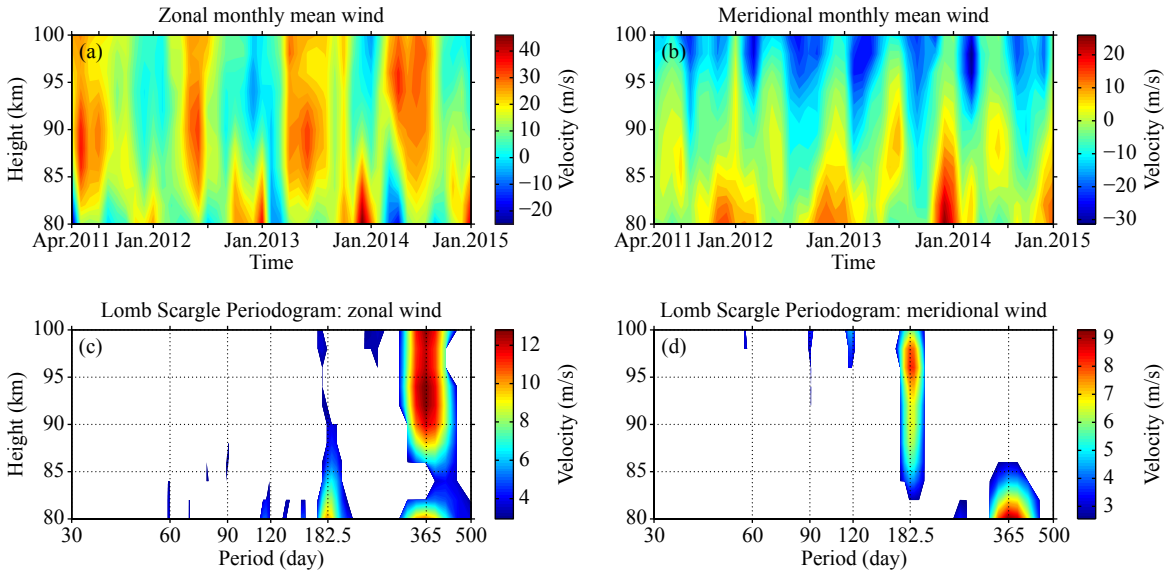

Figure 4. (a) Monthly mean zonal mean winds and (b) meridional mean winds from April 2011 to December 2014 over Kunming between altitudes of 80 and 100 km. Contour plot of the Lomb-Scargle periodogram spectra for the (c) daily mean zonal and (d) meridional winds between altitudes of 80 and 100 km; the Lomb-Scargle periodogram amplitudes are above the 95% confidence level.

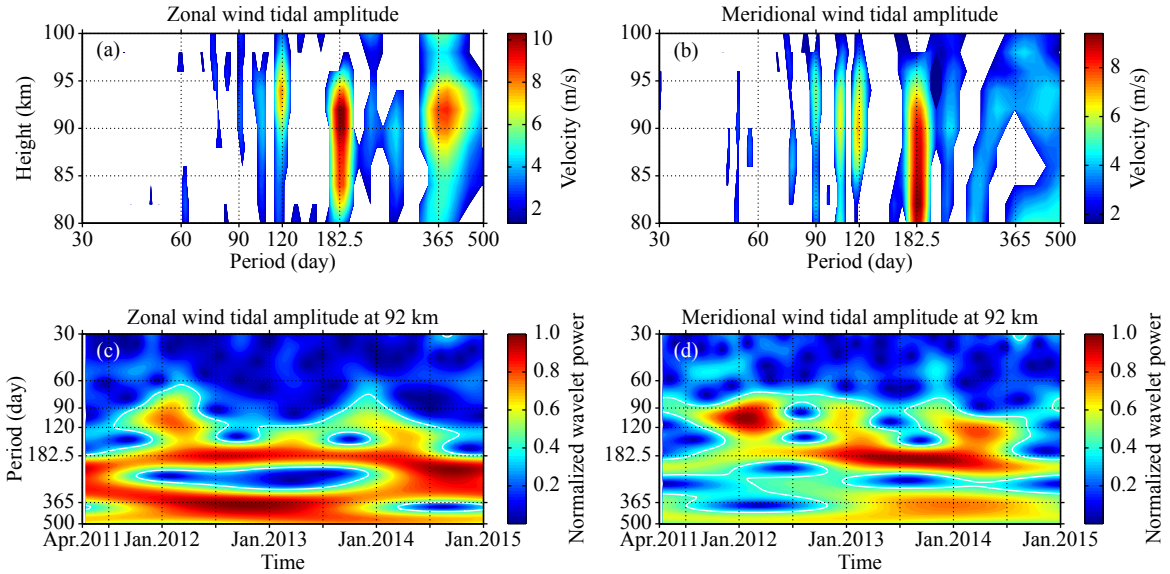

Figure 5. Contour plot of the Lomb-Scargle periodogram spectra for the (a) zonal wind diurnal tidal amplitudes and (b) meridional wind diurnal tidal amplitudes between altitudes of 80 and 100 km. The Lomb-Scargle periodogram amplitudes are higher than the 95% confidence level. The Morlet wavelet results at 92 km of the (c) zonal diurnal tidal amplitudes and (d) meridional diurnal tidal amplitudes.

at 94 km.

To verify the hypothesis that the quasi-90-day oscillation is excited by the upward propagation of tides from the lower atmosphere to the middle atmosphere, we calculate the tidal amplitude of zonal and meridional wind to examine the quasi-90-day oscillation. Figures 5a and 5b show the Lomb-Scargle periodograms of the zonal and meridional wind diurnal tidal amplitudes between altitudes of 80 and 100 km. The zonal wind diurnal amplitudes still show the weak quasi-90-day oscillation, but at the meridional wind diurnal amplitude, the quasi-90-day oscillation is prominent. The amplitudes of the quasi-90-day oscillation at the meridional wind diurnal amplitude are 3.82 m/s, 5.23 m/s and 4.59 m/s at 88 km, 92 km and 96 km, respectively; the amplitudes reach a maximum at approximately 94 km. In fact, the quasi-90-day oscillation is also observed at the meridional semidiurnal amplitudes (not shown here) from 88 km to 98 km, but exhibiting smaller amplitudes than the meridional diurnal amplitudes. Jiang GY et al. (2010) analyzed the wind tides obtained from a low latitude meteor radar (19.5°N, 109.1°E) and indicated that the meridional diurnal tide has larger amplitude than the zonal diurnal tide and that the diurnal tide is stronger than semidiurnal tide in the MLT region at the equator and low latitudes.

The Morlet wavelet result of the meridional wind diurnal amplitudes at 92 km in Figures 5c and 5d also proves that the quasi-90-day oscillation is a geophysical oscillation rather than a harmonic component of the AO or SAO in the MLT region. However, unlike the temperatures, the quasi-90-day oscillation in the meridional wind diurnal amplitudes appears in the winter and spring for approximately two cycles each year from 2011 to 2013, becomes weak in the winter of 2013 and is absent in the spring of 2014. We are further convinced by these results that the quasi-90-day oscillation is excited by upwardly propagating tides, but the energy generated by the breaking/dissipating of modulated tides may not be sufficient to drive a conspicuous quasi-90-day oscillation in the MLT wind mean flow.

5. Discussion

5.1 Source of Quasi-90-day Oscillation in Tides

Above, we presented the quasi-90-day oscillation in the temperatures and wind tides and confirmed that the quasi-90-day oscillation in the MLT is driven by upwardly propagated tides. Therefore, the question that arises from these results is as follows: *what is the source of these tides*?

At low latitudes, the atmospheric diurnal tides with a period of one day are excited by the absorption of solar radiation, latent heat release, and water vapor absorption of near-infrared (IR) radiation; moreover, they can propagate upward from the lower to middle atmosphere with strong amplitudes (Hagan and Forbes, 2002; Lieberman et al., 2003). In this study, the latent heat release was investigated as the possible source of the upwardly propagated tides from the lower atmosphere. Figure 6 shows the cross wavelet transform of the daily SABER nighttime temperature at 88 km and daily surface upward latent heat flux at (25.5°N, 103.5°E) from April 2011 to December 2014, obtained from the European Center for Medium-Range Weather Forecasting (ECWMF). The daily surface latent heat flux shows a domination of the AO. Therefore, we needed first to filter the AO component from the surface latent heat flux. The cross wavelet analysis in Figure 6 shows that the 90-day variabilities in SABER nighttime temperature and surface latent heat flux are correlated, with approximately two cycles per year from 2011 to 2013, but the correlation is absent in the winter of 2013 and the spring of 2014. Note that the quasi-90-day oscillation also appears to be synchronized with the meridional wind tides in the mesosphere (shown in Figure 5c) and the latent heat release in the troposphere. Huang KM et al. (2015) reported a quasi-27-day oscillation propagating from the troposphere to the mesosphere at low latitude and found that the latent heat release may not only modulate the tide but also excite similar short period oscillations in the lower atmosphere, and that these short period oscillations can propagate to the MLT region. However, as we mentioned above, the quasi-90-day oscillation is a long period oscillation that cannot propagate to the MLT from the lower atmosphere (Eckermann and Vincent, 1994). Therefore, we infer that the diurnal tides may be modulated by the 90-day variability of the latent heat release in the troposphere and then propagate upward and produce the quasi-90-day oscillation in the MLT region.

5.2 *In-situ* Source of Quasi-90-day Oscillation in MLT Temperature

The quasi-90-day oscillations in temperatures and wind tides are believed to be excited by the 90-day variability of upwardly propagated tides; however, this cannot explain why the quasi-90-day oscillation is weak in mean wind flow but evidently present in mean temperature. Fortunately, we were provided a clue for investigating the problem by the details shown in Figures 3e and 3f. We noted that the phases of the quasi-90-day oscillation below 60 km and near 90 km showed obvious phase reversals in the daytime temperature; moreover, these appear only in the daytime temperatures. Meanwhile, the amplitudes of the quasi-90-day oscillation below 60 km and near 90 km in the daytime are larger

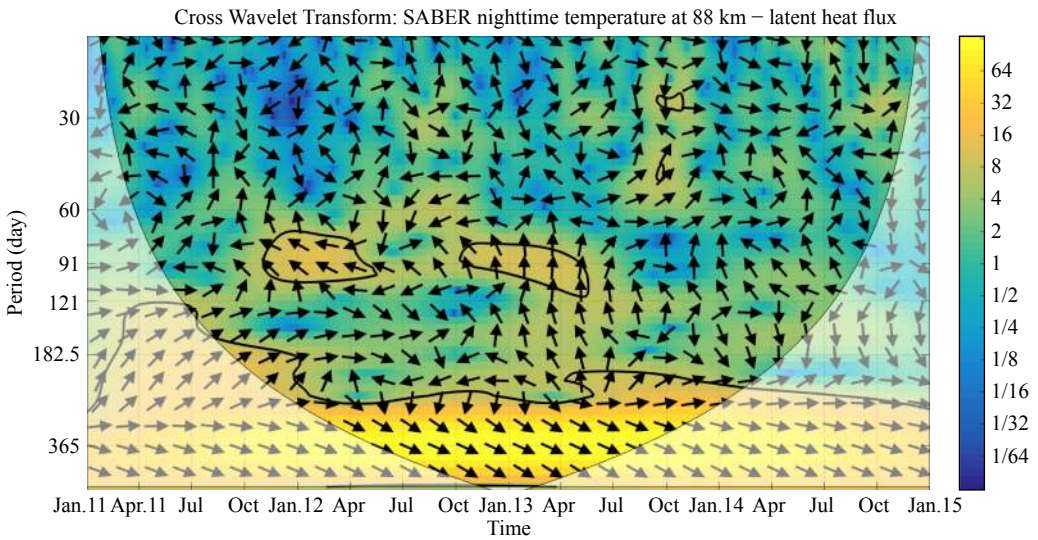

Figure 6. Cross wavelet transform of the SABER nighttime temperature at 88 km and daily surface upward latent heat flux at (25.5°N, 103.5°E) obtained from ECWMF from April 2011 to December 2014. The 95% significance level is shown as a thick contour. The relative phase relationship is shown as arrows (with in-phase pointing right, anti-phase pointing left, and temperature leading ozone by 90° pointing straight up).

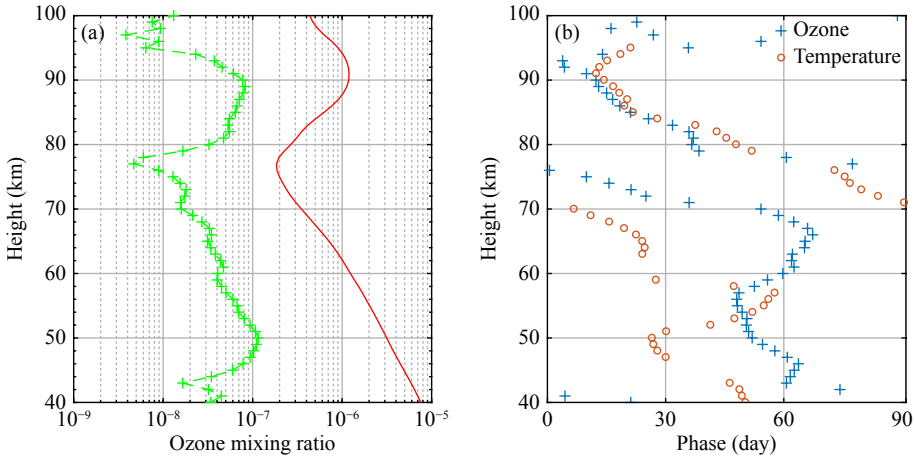

Figure 7. (a) Height profiles of the averaged daytime O_3 (red solid line) and the amplitude of the quasi-90-day oscillation in daytime O_3 (green plus signs) and (b) phase-height profiles of the quasi-90-day oscillation for the SABER daytime O_3 and temperature from 40 to 100 km over Kunming.

than in the nighttime.

Figure 7a shows the height profiles of daytime O_3 (red solid line) and the amplitude of the quasi-90-day oscillation in daytime O_3 over Kunming. The O_3 maximum appears in the stratosphere near 35 km over Kunming (not show here). As shown in Figure 7a, the O_3 shows a decrease as the altitude increases below 75 km, and then shows an increase as the altitude increases above 75 km. The secondary O_3 maximum is present in the mesopause region (near 90 km). The amplitudes of the quasi-90-day oscillation in O_3 also show peaks below 60 km and near 90 km. As we mentioned above, as well as show in Figure 7b, the phase of the quasi-90-day oscillation in daytime temperature shows a reversal below 60 km and near 90 km. Therefore, we infer that the phase reversal and larger amplitude in the daytime quasi-90-day oscillation temperature may be related to O_3 absorption of UV radiation.

The phase reversal of the quasi-90-day oscillation in daytime temperature below 60 km coincides with the height of the maximum heating rate attributed to the stratospheric O_3 absorption. Here we use daytime O_3 and temperatures observed by Aura/MLS instead of the SABER measurements to examine the relationship between them because SABER stopped observing at noon for approximately two hours, and this creates approximately 20 days of data gaps in SABER daytime observations. As we can see from Figure 8, the cross wavelet analysis of the MLS daytime O_3 and temperatures near 60 km shows that the daytime O_3 and temperatures have strong correlation with the period of 90 days. The cross wavelet analysis also shows that the variations of the daytime temperature and O_3 are roughly in anti-phase because low temperatures accelerate the formation and inhibit the loss of O_3 and inhibit its the loss, and vice-versa for high temperatures (Smith and Marsh, 2005). Note that the quasi-90-day oscillation is stronger than AO and SAO in daytime O_3 and temperature. Studies indicated that the O_3 absorption of UV radiation in the stratosphere and the lower mesosphere (below 60 km) is considered to be another source of the propagating diurnal tides, except for the

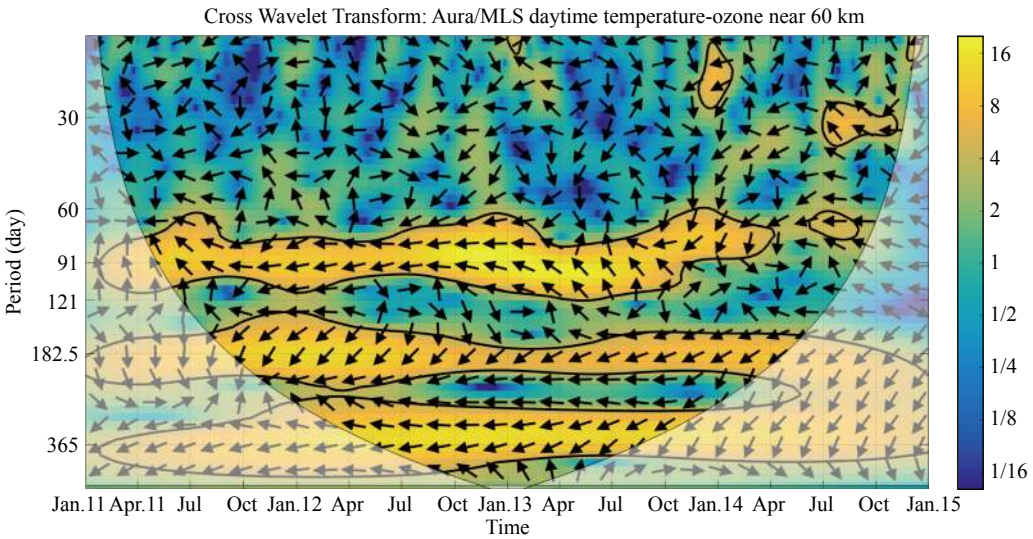

Figure 8. Same as Figure 6, but for the Aura/MLS day temperatures and O_3 at a pressure level of 0.146 hPa (near 60 km).

latent heat release and water vapor heating in the troposphere (Hagan, 1996; Lieberman et al., 2003).

Smith et al. (2010) noted that the diurnal variations of upper mesosphere O_3 are driven by diurnal tides. Pancheva et al. (2014) found non-migrating tidal variations in mesosphere O_3 and considered these variations to be the response of the mesosphere O_3 to non-migrating tides propagating upward from the lower atmosphere. As we can see in Figure 7b, the phase of the 90-day oscillations in daytime temperature and O_3 match well above 75 km, which indicates that the 90-day variation of upwardly propagated tides generates not only the 90-day variability of the daytime temperature in the mesosphere but also a similar variation of daytime O_3.

The SABER O_3 data over the Kunming meteor radar were employed to investigate the effects of O_3 absorption of UV radiation in response to the quasi-90-day oscillation of temperature. Figure 9a shows the SABER nighttime O_3 at 88 km from April 2011 to December 2014 over Kunming. Because the nighttime O_3 shows a strong domination of SAO, we needed first to filter the SAO component from nighttime O_3. The Morlet wavelet result of the filtered SABER nighttime O_3 in Figure 9b shows that the 90-day variability of O_3 presents mainly in the first half of the year, in approximately two cycles. Notably, the 90-day variability of SABER nighttime O_3 at 88 km occurs simultaneously with the quasi-90-day oscillation in the Kunming meteor radar temperature (shown in Figure 2b) and SABER temperature (shown in Figure 2c). O_3 is one of the principal absorbers of UV radiation in the mesopause (Smith and Marsh, 2005). Thus, we infer that the 90-day variability of daytime O_3 alters the heating rate and temperature directly, which is an *in situ* source of generating the quasi-90-day oscillation in MLT temperature. The quasi-90-day oscillation in daytime temperature has a larger amplitude than that in nighttime temperature; therefore, we observed directly a significant quasi-90-day oscillation in the daily mean temperature.

6. Summary

In this paper, we present multiple observations of quasi-90-day oscillations in the MLT region from April 2011 to December 2014 and investigate the excitation source of these observations. The quasi-90-day oscillation in temperatures obtained from the Kunming meteor radar (25.6°N, 103.8°E) and SABER is a dominant seasonal variation that has two regular cycles in the first half of each year. The amplitudes and phase of the quasi-90-day oscillation in the SABER temperatures show a similar feature of upwardly propagated diurnal tides that have a vertical wavelength of ~20 km above 70 km. Moreover, the meridional wind tides in the MLT region, calculated from the Kunming meteor radar horizontal winds, also present dominant quasi-90-day oscillations with two wave cycles in each year. These observations reveal that the quasi-90-day oscillation in the MLT region is related to the 90-day variability of upwardly propagated diurnal tides.

To trace the origin of the 90-day variability of diurnal tides, we analyzed the surface latent heat flux obtained from ECMWF and found that the surface latent heat flux shows 90-day variability. This result reveals that the variability of diurnal tides should be modulated by the 90-day availability of latent heat released in the lower atmosphere that then propagates upward and generates the quasi-90-day oscillation in the MLT region. The daytime O_3 in the MLT region also shows 90-day variability corresponding to the quasi-90-day oscillation in daytime temperature. The 90 day variability of O_3 in the middle atmosphere is considered to be driven by the similar variability of upwardly propagated diurnal tides. Conversely, the 90 day variability of daytime O_3 directly alters the heating rate and temperature, which is an *in situ* source of generating quasi-90-day oscillations in daytime temperature. The significance of the present results lies in showing that the quasi-90-day oscillation is an example of coupling between the lower and middle atmosphere through upwardly propagated tides.

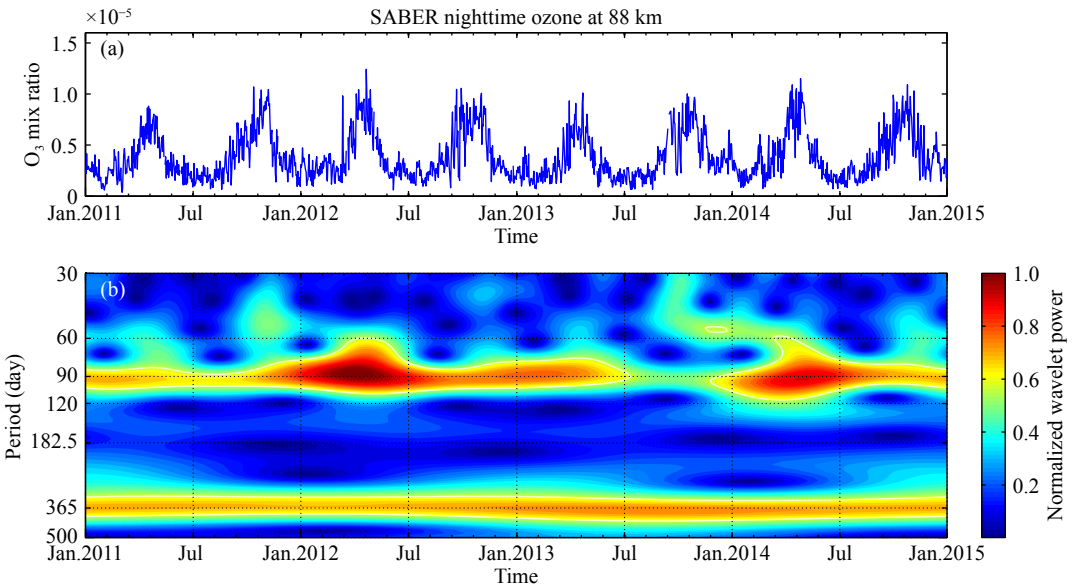

Figure 9. (a) SABER nighttime O_3 from 2011 to 2014 at 88 km over Kunming; (b) Morlet wavelet results of the SABER nighttime O_3 from 2011 to 2014.

Acknowledgments

We acknowledge the Kunming Atmospheric Radar Facility (KARF) for providing the meteor radar data. The KARF belongs to and is operated by the China Research Radar Institute of Radiowave Propagation (CRIRP). We thank the NASA TIMED/SABER teams for providing free access to their data. The ECMWF ERA-Interim data used in this study were downloaded from the ECMWF data server at http://apps.ecmwf.int/datasets/data/interim-full-daily/. The GSWM-09 tide data were obtained from http://www.hao.ucar.edu/modeling/gswm/. Aura/MLS data are available from http://disc.sci.gsfc.nasa.gov/Aura/data-holdings/MLS.

This work is supported by Project (KJCX2-EW-J01, KZZD-EW-0101) of the Chinese Academy of Sciences, the National Natural Science Foundation of China (41322029, 41474129, 41421063 and 41804147), the National Basic Research Program of China (2012CB825605), the Youth Innovation Promotion Association of the Chinese Academy of Sciences (2011324), and the Fundamental Research Funds for the Central Universities, the open research project of Chinese Academy of Sciences Large Research Infrastructures, and the Chinese Meridian Project, the Open Research Program of National Key Laboratory of Electromagnetic Environment of the China Research Institute of Radiowave Propagation.

References

Eckermann, S. D., and Vincent, R. A. (1994). First observations of intraseasonal oscillations in the equatorial mesosphere and lower thermosphere. *Geophys. Res. Lett.*, *21*(4), 265–268. https://doi.org/10.1029/93GL02835

Eckermann, S. D., Rajopadhyaya, D. K., and Vincent, R. A. (1997). Intraseasonal wind variability in the equatorial mesosphere and lower thermosphere: Long-term observations from the central pacific. *J. Atmos. Sol. Terr. Phys.*, *59*(6), 603–627. https://doi.org/10.1016/S1364-6826(96)00143-5

Gasperini, F., Hagan, M. E., and Zhao, Y. (2017). Evidence of tropospheric 90 day oscillations in the thermosphere. *Geophys. Res. Lett.*, *44*(20), 10125–10133. https://doi.org/10.1002/2017GL075445

Grinsted, A., Moore, J. C., and Jevrejeva, S. (2004). Application of the cross wavelet transform and wavelet coherence to geophysical time series. *Nonlin. Processes Geophys.*, *11*(5-6), 561–566. https://doi.org/10.5194/npg-11-561-2004

Guharay, A., Sekar, R., Venkat Ratnam, M., and Batista, P. P. (2012). Characteristics of the intraseasonal oscillations in the lower and middle atmosphere over Gadanki. *J. Atmos. Sol. Terr. Phys.*, *77*, 167–173. https://doi.org/10.1016/j.jastp.2011.12.016

Guharay, A., Batista, P. P., Clemesha, B. R., Sarkhel, S., and Buriti, R. A. (2014). Investigation of the intraseasonal oscillations over a Brazilian equatorial station: a case study. *Earth Planets Space*, *66*, 145. https://doi.org/10.1186/s40623-014-0145-3

Gurubaran, S., and Rajaram, R. (1999). Long-term variability in the mesospheric tidal winds observed by MF radar over Tirunelveli (8.7°N, 77.8°E). *Geophys. Res. Lett.*, *26*(8), 1113–1116. https://doi.org/10.1029/1999GL900171

Hagan, M. E., Forbes, J. M., and Vial, F. (1995). On modeling migrating solar tides. *Geophys. Res. Lett.*, *22*(8), 893–896. https://doi.org/10.1029/95GL00783

Hagan, M. E. (1996). Comparative effects of migrating solar sources on tidal signatures in the middle and upper atmosphere. *J. Geophys. Res.*, *101*(D16), 21213–21222. https://doi.org/10.1029/96JD01374

Hagan, M. E., and Forbes, J. M. (2002). Migrating and nonmigrating diurnal tides in the middle and upper atmosphere excited by tropospheric latent heat release. *J. Geophys. Res.*, *107*(D24), ACL 6-1–ACL 6-15. https://doi.org/10.1029/2001JD001236

Hocking, W. K. (1999). Temperatures using radar-meteor decay times. *Geophys. Res. Lett.*, *26*(21), 3297–3300. https://doi.org/10.1029/1999GL003618

Hocking, W. K., Fuller, B., and Vandepeer, B. (2001). Real-time determination of meteor-related parameters utilizing modern digital technology. *J. Atmos. Sol. Terr. Phys.*, *63*(2-3), 155–169. https://doi.org/10.1016/S1364-6826(00)00138-3

Holdsworth, D. A., Reid, I. M., and Cervera, M. A. (2004). Buckland Park all-sky interferometric meteor radar. *Radio Science*, *39*, RS5009. https://doi.org/10.1029/2003RS003014

Holdsworth, D. A., Morris, R. J., Murphy, D. J., Reid, I. M., Burns, G. B., and French, W. J. R. (2006). Antarctic mesospheric temperature estimation using the Davis mesosphere-stratosphere-troposphere radar. *J. Geophys. Res.*, *111*(D5), D05108. https://doi.org/10.1029/2005JD006589

Huang, K. M., Liu, A. Z., Zhang, S. D., Yi, F., Huang, C. M., Gan, Q., Gong, Y., Zhang, Y. H., and Wang, R. (2015). Observational evidence of quasi-27-day oscillation propagating from the lower atmosphere to the mesosphere over 20°N. *Ann. Geophys.*, *33*(10), 1321–1330. https://doi.org/10.5194/angeo-33-1321-2015

Isoda, F., Tsuda, T., Nakamura, T., Vincent, R. A., Reid, I. M., Achmad, E., Sadewo, A., and Nuryanto, A. (2004). Intraseasonal oscillations of the zonal wind near the mesopause observed with medium-frequency and meteor radars in the tropics. *J. Geophys. Res.*, *109*(D21), D21108. https://doi.org/10.1029/2003JD003378

Jiang, G. Y., Xu, J. Y., Shi, J. K., Yang, G. T., Wang, X., and Yan, C. X. (2010). The first observation of the atmospheric tides in the mesosphere and lower thermosphere over Hainan, China. *Chin. Sci. Bull.*, *55*(11), 1059–1066. https://doi.org/10.1007/s11434-010-0084-8

Kumar, K. K., Antonita, T. M., Ramkumar, G., Deepa, V., Gurubaran, S., and Rajaram, R. (2007). On the tropospheric origin of Mesosphere Lower Thermosphere region intraseasonal wind variability. *J. Geophys. Res.*, *112*(D7), D07109. https://doi.org/10.1029/2006JD007962

Li, N., Chen, J. S., Ding, Z. H., and Zhao, Z. W. (2015). Mean winds observed by the Kunming MF radar in 2008-2010. *J. Atmos. Sol. -Terr. Phys.*, *122*, 58–65. https://doi.org/10.1016/j.jastp.2014.10.011

Li, T., Liu, A. Z., Lu, X., Li, Z. H., Franke, S. J., Swenson, G. R., and Dou, X. K. (2012). Meteor-radar observed mesospheric semi-annual oscillation (SAO) and quasi-biennial oscillation (QBO) over Maui, Hawaii. *J. Geophys. Res.*, *117*(D5), D05130. https://doi.org/10.1029/2011JD016123

Lieberman, R. S. (1998). Intraseasonal variability of high-resolution Doppler imager winds in the equatorial mesosphere and lower thermosphere. *J. Geophys. Res.*, *103*(D10), 11221–11228. https://doi.org/10.1029/98JD00532

Lieberman, R. S., Ortland, D. A., and Yarosh, E. S. (2003). Climatology and interannual variability of diurnal water vapor heating. *J. Geophys. Res.*, *108*(D3), 4123. https://doi.org/10.1029/2002JD002308

Lomb, N. R. (1976). Least-squares frequency analysis of unequally spaced data. *Astrophys. Space Sci.*, *39*(2), 447–462. https://doi.org/10.1007/BF00648343

Lu, X., Liu, A. Z., Oberheide, J., Wu, Q., Li, T., Li, Z. H., Swenson, G. R., and Franke, S. J. (2011). Seasonal variability of the diurnal tide in the mesosphere and lower thermosphere over Maui, Hawaii (20.7°N, 156.3°W). *J. Geophys. Res.*, *116*(D17), D17103. https://doi.org/10.1029/2011JD015599

Luo, Y., Manson, A. H., Meek, C. E., Igarashi, K., and Jacobi, C. (2001). Extra long period (20-40 day) oscillations in the mesospheric and lower thermospheric winds: observations in Canada, Europe and Japan, and considerations of possible solar influences. *J. Atmos. Sol. Terr. Phys.*, *63*(9), 835–852. https://doi.org/10.1016/S1364-6826(00)00206-6

Madden, R. A., and Julian, P. R. (1971). Detection of a 40-50 day oscillation in the zonal wind in the tropical Pacific. *J. Atmos. Sci.*, *28*(5), 702–708. https://doi.org/10.1175/1520-0469(1971)028<0702:DOADOI>2.0.CO;2

Madden, R. A., and Julian, P. R. (1972). Description of global-scale circulation cells in the tropics with a 40-50 day period. *J. Atmos. Sci.*, *29*(6), 1109–1123. https://doi.org/10.1175/1520-0469(1972)029<1109:DOGSCC>2.0.CO;2

Miyoshi, Y., and Fujiwara, H. (2006). Excitation mechanism of intraseasonal oscillation in the equatorial mesosphere and lower thermosphere. *J. Geophys. Res.*, *111*(D14), D14108. https://doi.org/10.1029/2005JD006993

Mukhtarov, P., Pancheva, D., and Andonov, B. (2009). Global structure and seasonal and interannual variability of the migrating diurnal tide seen in the SABER/TIMED temperatures between 20 and 120 km. *J. Geophys. Res.*, *114*(A2), A02309. https://doi.org/10.1029/2008JA013759

Pancheva, D., Mitchell, N. J., Younger, P. T., and Muller, H. G. (2003). Intra-

seasonal oscillations observed in the MLT region above UK (52°N, 2°W) and ESRANGE (68°N, 21°E). *Geophys. Res. Lett.*, *30*(21), 2084. https://doi.org/10.1029/2003GL017809

Pancheva, D., Mukhtarov, P., and Smith, A. K. (2014). Nonmigrating tidal variability in the SABER/TIMED mesospheric ozone. *Geophys. Res. Lett.*, *41*(11), 4059–4067. https://doi.org/10.1002/2014GL059844

Rao, R. K., Gurubaran, S., Sathishkumar, S., Sridharan, S., Nakamura, T., Tsuda, T., Takahashi, H., Batista, P. P., Clemesha, B. R., … Mitchell, N. J. (2009). Longitudinal variability in intraseasonal oscillation in the tropical mesosphere and lower thermosphere region. *J. Geophys. Res.*, *114*(D19), D19110. https://doi.org/10.1029/2009JD011811

Reid, I. M., Spargo, A. J., and Woithe, J. M. (2014). Seasonal variations of the nighttime O(1S) and OH (8-3) airglow intensity at Adelaide, Australia. *J. Geophys. Res. Atmos.*, *119*(11), 6991–7013. https://doi.org/10.1002/2013JD020906

Scargle, J. D. (1982). Studies in astronomical time series analysis. II- Statistical aspects of spectral analysis of unevenly spaced data. *Astrophys. J.*, *263*, 835–853. https://doi.org/10.1086/160554

Shepherd, M. G., Evans, W. F. J., Hernandez, G., Offermann, D., and Takahashi, H. (2004). Global variability of mesospheric temperature: Mean temperature field. *J. Geophys. Res.*, *109*(D24), D24117. https://doi.org/10.1029/2004JD005054

Smith, A. K., and Marsh, D. R. (2005). Processes that account for the ozone maximum at the mesopause. *J. Geophys. Res.*, *110*(D23), D23305. https://doi.org/10.1029/2005JD006298

Smith, A. K., Marsh, D. R., Mlynczak, M. G., and Mast, J. C. (2010). Temporal variations of atomic oxygen in the upper mesosphere from SABER. *J. Geophys. Res.*, *115*(D18), D18309. https://doi.org/10.1029/2009JD013434

Sridharan, S., Tsuda, T., and Gurubaran, S. (2007). Radar observations of long-term variability of mesosphere and lower thermosphere winds over Tirunelveli (8.7°N, 77.8°E). *J. Geophys. Res.*, *112*(D23), D23105. https://doi.org/10.1029/2007JD008669

Torrence, C., and Compo, G. P. (1998). A practical guide to wavelet analysis. *Bull. Amer. Meteor. Soc.*, *79*(1), 61–78. https://doi.org/10.1175/1520-0477(1998)079<0061:APGTWA>2.0.CO;2

Vincent, R. A., Kovalam, S., Fritts, D. C., and Isler, J. R. (1998). Long-term MF radar observations of solar tides in the low-latitude mesosphere: Interannual variability and comparisons with the GSWM. *J. Geophys. Res.*, *103*(D8), 8667–8683. https://doi.org/10.1029/98JD00482

Xu, J. Y., Smith, A. K., Yuan, W., Liu, H. L., Wu, Q., Mlynczak, M. G., and Russell III, J. M. (2007). Global structure and long-term variations of zonal mean temperature observed by TIMED/SABER. *J. Geophys. Res.*, *112*(D24), D24106. https://doi.org/10.1029/2007JD008546

Xue, X. H., Dou, X. K., Lei, J., Chen, J. S., Ding, Z. H., Li, T., Gao, Q., Tang, W. W., Cheng, X. W., and Wei, K. (2013). Lower thermospheric-enhanced sodium layers observed at low latitude and possible formation: Case studies. *J. Geophys. Res.*, *118*(5), 2409–2418. https://doi.org/10.1002/jgra.50200

Yang, C., Li, T., Smith, A. K., and Dou, X. (2017). The response of the southern hemisphere middle atmosphere to the madden-julian oscillation during austral winter using the specified-dynamics whole atmosphere community climate model. *J. Climate*, *30*(20), 8317–8333. https://doi.org/10.1175/JCLI-D-17-0063.1

Yang, C. Y., Smith, A. K., Li, T., and Dou, X. K. (2018). The effect of the Madden-Julian oscillation on the mesospheric migrating diurnal tide: A study using SD-WACCM. *Geophys. Res. Lett.*, *45*(10), 5105–5114. https://doi.org/10.1029/2018GL077956

Yi, W., Xue, X. H., Chen, J. S., Dou, X. K., Chen, T. D., and Li, N. (2016). Estimation of mesopause temperatures at low latitudes using the Kunming meteor radar. *Radio Sci.*, *51*(3), 130–141. https://doi.org/10.1002/2015RS005722

Yi, W., Xue, X. H., Reid, I. M., Younger, J. P., Chen, J. S., Chen, T. D., and Li, N. (2018). Estimation of mesospheric densities at low latitudes using the Kunming meteor radar together with SABER temperatures. *J. Geophys. Res.*, *123*(4), 3183–3195. https://doi.org/10.1002/2017JA025059

Zhang, C. D. (2005). Madden-Julian oscillation. *Rev. Geophys.*, *43*(2), RG2003. https://doi.org/10.1029/2004RG000158

Zhang, X. L., Forbes, J. M., Hagan, M. E., Russell III, J. M., Palo, S. E., Mertens, C. J., and Mlynczak, M. G. (2006). Monthly tidal temperatures 20-120 km from TIMED/SABER. *J. Geophys. Res.*, *111*(A10), A10S08. https://doi.org/10.1029/2005JA011504